

RESEARCH ARTICLE | AUGUST 16 2024

Substituent effects on first generation photochemical molecular motors probed by femtosecond stimulated Raman



Special Collection: [Time-resolved Vibrational Spectroscopy](#)

Palas Roy ; Andy S. Sardjan ; Wojciech Danowski ; Wesley R. Browne ; Ben L. Feringa ; Stephen R. Meech



J. Chem. Phys. 161, 074504 (2024)

<https://doi.org/10.1063/5.0216442>



28 August 2024 09:08:09



The Journal of Chemical Physics

Special Topic:
Dynamic Exciton for Materials, Biology
and Energy Conversion

Guest Editors: Hiroshi Imahori, Prashant Kamat, Hironori Kaji, Yasuhiro Kobori, Kiminori Maeda, Michael R. Wasielewski
JCP Editors: Tianquan (Tim) Lian, Renee Frontiera, Jennifer Ogilvie, Qiang Shi

[Submit Today!](#)



Substituent effects on first generation photochemical molecular motors probed by femtosecond stimulated Raman

Cite as: J. Chem. Phys. 161, 074504 (2024); doi: 10.1063/5.0216442

Submitted: 29 April 2024 • Accepted: 15 July 2024 •

Published Online: 16 August 2024



View Online



Export Citation



CrossMark

Palas Roy,^{1,2} Andy S. Sardjan,³ Wojciech Danowski,^{4,5} Wesley R. Browne,³ Ben L. Feringa,^{4,a)} and Stephen R. Meech^{1,a)}

AFFILIATIONS

¹School of Chemistry, University of East Anglia, Norwich NR4 7TJ, United Kingdom

²School of Basic Sciences, Indian Institute of Technology Bhubaneswar, Bhubaneswar, Odisha 752050, India

³Molecular Inorganic Chemistry, Stratingh Institute for Chemistry, Faculty of Science and Engineering, University of Groningen, 9747AG Groningen, The Netherlands

⁴Centre for Systems Chemistry, Stratingh Institute for Chemistry, Faculty of Science and Engineering, University of Groningen, 9747AG Groningen, The Netherlands

⁵Faculty of Chemistry, University of Warsaw, Pasteura 1, 02-093 Warsaw, Poland

Note: This paper is part of the JCP Special Topic on Time-resolved Vibrational Spectroscopy 2023.

a) Authors to whom correspondence should be addressed: b.l.feringa@rug.nl and s.meech@uea.ac.uk

ABSTRACT

Unidirectional photochemical molecular motors can act as a power source for molecular machines. The motors operate by successive excited state isomerization and ground state helix inversion reactions, attaining unidirectionality from an interplay of steric strain and stereochemistry. Optimizing the yield of the excited state isomerization reaction is an important goal that requires detailed knowledge of excited state dynamics. Here, we investigate the effect of electron withdrawing and donating substituents on excited state structure and ultrafast dynamics in a series of newly synthesized first generation photochemical molecular motors. All substituents red-shift the absorption spectra, while some modify the Stokes shift and render the fluorescence quantum yield solvent polarity dependent. Raman spectra and density functional theory calculations reveal that the stretching mode of the C=C “axle” in the electronic ground state shows a small red-shift when conjugated with electron withdrawing substituents. Ultrafast fluorescence measurements reveal substituent and solvent polarity effects, with the excited state decay being accelerated by both polar solvent environment and electron withdrawing substituents. Excited state structural dynamics are investigated by fluorescence coherence spectroscopy and femtosecond stimulated Raman spectroscopy. The time resolved Raman measurements are shown to provide structural data specifically on the Franck–Condon excited state. The C=C localized modes have a different substituent dependence compared to the ground state, with the unsubstituted motor having the most red-shifted mode. Such measurements provide valuable new insights into pathways to optimize photochemical molecular motor performance, especially if they can be coupled with high-quality quantum molecular dynamics calculations.

Published under an exclusive license by AIP Publishing. <https://doi.org/10.1063/5.0216442>

INTRODUCTION

Unidirectional photochemical molecular motors (PMMs) based on sterically overcrowded alkenes undergo two-step photochemically and thermally induced *cis*–*trans* isomerization reactions.^{1–8} Unidirectionality is imposed by a combination of steric and stereochemical factors. Previous studies on unsubstituted

motors show that light absorption places the motor in an unstable Franck–Condon state, which is emissive in nature and thus labeled a bright state (Fig. 1). Excitation to the bright state is localized on the sterically strained ethylenic “axle,” reducing its bond order in the excited electronic state.⁹ Due to the steric repulsion, this bright state undergoes a unidirectional ultrafast (typically <200 fs) relaxation on the excited state potential energy surface to populate

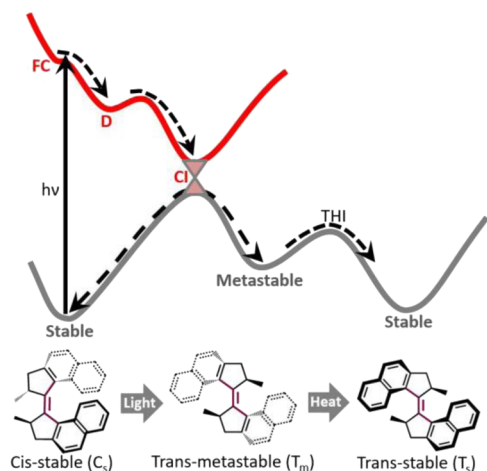


FIG. 1. Generic potential energy diagram for photoconversion of a first generation motor and its associated reactions. FC, Franck–Condon state; D, dark state; THI, Thermal Helix Inversion; and CI, conical intersection region to ground electronic state.

an intermediate state with a substantially reduced transition dipole moment, called a dark state.^{10–14} This dark state relaxes on a picosecond timescale through a conical intersection (CI) to populate either a metastable (at room temperature) product isomer or the original ground state (Fig. 1). The metastable product then undergoes a unidirectional thermal helix inversion (THI) to form the more stable product isomer, which again has a sterically strained double bond axle. Absorption of a second photon gives rise to a second excited state isomerization and ground state helix inversion, which necessarily proceed in the same direction as the first, to yield one complete rotation.

The efficiency of PMMs is a function of the rate of ground state helix inversion (the rate determining step) and the quantum yield of the ultrafast excited state isomerization.¹⁵ Tuning the molecular structure and number of stereocenters around the C=C axle led to second and third generations of PMMs that show different efficiencies.^{7,12,16–19} First generation motors containing two stereocenters had photoisomerization yields reaching 60% in some cases, but low rates of helix inversion. The second and third generation motors (with one chiral and one pseudo-asymmetric center, respectively) showed significantly lower isomerization yields but with dramatically higher rates of helix inversion. Thus, while synthetic variation successfully controlled the rate of the rate determining ground state helix inversion, controlling the photoisomerization yield has proven more challenging.

The excited state dynamics and the nature of the bright and dark states of all three generations of PMMs have been investigated using several time-resolved spectroscopic techniques and quantum chemical calculations.^{9,11–14,20–35} Increasing solvent viscosity was found to significantly slow the dynamics of dark state decay, while bright state dynamics remain largely unchanged.^{12,21} It was observed that the lifetime of the dark state in a first-generation PMM is also a strong function of solvent polarity.²³ This dependence was rationalized by assuming polar solvent stabilization of a charge transfer configuration arising from sudden polarization

in the dark state, resulting in a lower barrier on the pathway to the CI. Inspired by this model, electron donating and withdrawing groups were attached in conjugation with the C=C motor “axle” in an effort to control this polar character, and thus the dynamics of the dark state and ultimately the isomerization yield. Recently, we have shown that simultaneous location of electron donating and withdrawing substituents (a “push–pull motor”) in conjugation with the “axle” double bond in a first generation PMM allowed a remarkable degree of solvent control over the photoisomerization yield.³⁶ In this work, we probe the photophysics of four substituted first generation PMMs, three of them studied for the first time (Fig. 2), and compare their spectra and dynamics with those of the parent and push–pull motors previously investigated. In particular, we apply ultrafast fluorescence to probe population decay and fluorescence coherence spectroscopy and femtosecond stimulated Raman spectroscopy (FSRS) to recover excited state vibrational spectra between near zero and 1700 cm^{-1} .

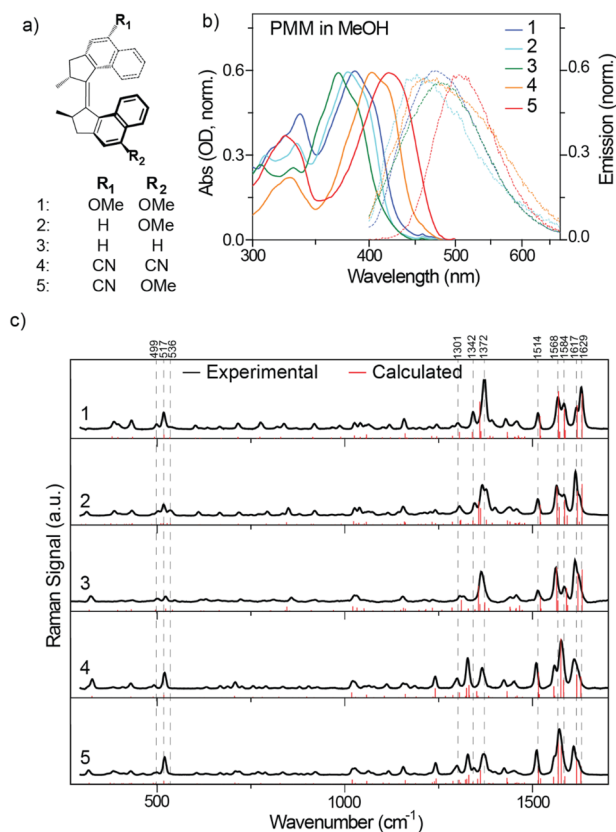


FIG. 2. (a) Chemical structure of all the five motors studied and (b) their corresponding steady-state absorption (solid) and emission (dashed, excited at 390 nm) spectra. (c) Experimental (black solid lines) and calculated (red vertical lines) steady-state off-resonance Raman of the five motor derivatives in the solid state. Raman excitation at 532 nm. The black dashed lines (labeled with the corresponding wavenumber) are a guide to eye to show the shift in Raman peak position in different motor derivatives.

RESULTS AND DISCUSSION

Steady-state electronic spectroscopy

The steady-state absorption and emission spectra for the five motor derivatives [Fig. 2(a)] dissolved in the polar solvent methanol ($\epsilon = 32.7$) are shown in Fig. 2(b) (the corresponding spectra in the apolar solvent cyclohexane, $\epsilon = 2.0$, are shown in Fig. S3). The new motors (1, 2, and 4) contain symmetrical substitution with two electron-donating methoxy (1) or two electron-withdrawing cyano (4) substituents or are asymmetrically substituted with one methoxy (2, the corresponding single cyano derivative could not be prepared in sufficient yield and purity) or one methoxy and one cyano group (5); synthetic procedures are described in the [supplementary material](#). The absorption maxima for motors 1–5 are presented in Table I. The spectra for all substituted PMMs are red-shifted from the unsubstituted parent 3, presumably as a result of either stabilization of the excited state or destabilization of the ground state. The previously studied push–pull motor 5 has the most red-shifted absorption. Despite the spectral shifts, the spectra all have similar shapes and molar absorptivity, corresponding to a π – π^* transition. Quantum chemical calculations for 3 revealed this transition to be localized on the ethylenic axle of the motor.⁹ The corresponding emission spectra are weak and broad [Fig. 2(b)]. These data provided the Stokes shift (expressed in wavenumbers; see Table I), where it is seen that 3 has the largest overall Stokes shift, while 4 shows the largest change between apolar cyclohexane and polar methanol. Significantly, 1–4 all have a larger Stokes loss in apolar than in polar solvent. This solvent dependence suggests that the origin of the Stokes loss lies in solvent induced changes in the profile of the electronic spectra, rather than a change in permanent dipole moment between ground and excited states due to stabilization by polar solvation. The exception is the push–pull motor 5 described earlier,³⁶ with the Stokes loss here indicating a more polar character in the excited state due to the push–pull substitution. Table I also shows a general trend toward a lower quantum yield of fluorescence in the polar solvent methanol, which is consistent with earlier studies of 3 and 5. In that case, this effect of solvent polarity was assigned to a reduced barrier to the CI in the excited state PES.^{21,23}

This effect is particularly large for 4, which also had an anomalously large decrease in Stokes shift in the polar solvent, suggesting a significant solvent perturbation to the excited state PES in this case.

Ground-state Raman spectroscopy

The steady-state Raman spectra of all five derivatives were recorded in the solid state under non-resonant (or pre-resonant) conditions [λ_{exc} 532 nm, Fig. 2(c)], to probe the influence of substituents on the ground state structure of PMMs. All derivatives show Raman active modes in the region of 1500–1600 and 1200–1400 cm^{-1} . In addition, all five motors show a moderate intensity in the low wavenumber region (500–550 cm^{-1}). All spectra show variation in terms of relative intensity and wavenumber, indicating a significant effect of substituent on Raman activity. Ground-state density functional theory (DFT, rb3lyp/TZVP) calculations of the Raman active modes were performed using Gaussian 16³⁷ [shown in Fig. 2(c)] to assign these spectra (see the [supplementary material](#) for coordinates). Experimental and calculated spectra match well in the region 1000–1700 cm^{-1} for all the derivatives, but the calculations predict less activity in the low wavenumber region than is observed experimentally, although there is good agreement in band position. The calculations suggest assignment of the highest wavenumber modes (near 1615–1630 cm^{-1}) to stretching of the ethylenic C=C axle coupled to either a symmetric or asymmetric ring C=C stretch (displacements shown in the [supplementary material](#), Fig. S1). The 1629 and 1617 cm^{-1} bands in motor 1 are the most blue-shifted (higher wavenumber) of the derivatives, with the bands for the others red-shifting in the order $2 < 3 < 4 < 5$, although the overall shift is small (the entire range is from 1629 cm^{-1} (1) to 1622 cm^{-1} (5) in the highest wavenumber band). Similarly, DFT leads us to assign the next highest frequency modes to symmetric and asymmetric C=C ring stretches (see displacement in the [supplementary material](#), Fig. S1), e.g., at 1584 and 1568 cm^{-1} in motor 1 (again the most blue-shifted). These modes also undergo a red-shift on substitution, again in the order $2 < 3 < 4 < 5$. Based on these observations, we conclude that electron donating substituents lead to a slightly stronger C=C bond, while electron withdrawing ones have the opposite effect. The

TABLE I. The absorption and emission maxima, the corresponding Stokes shift, and the fluorescence quantum yield (QY) of the PMM derivatives are tabulated.

PMM	Solvent	Absorption maxima (nm)	Emission maxima (nm)	Stokes shift (cm^{-1})	Fluorescence quantum yield (%)
1	MeOH	386	476	4898	0.96
	CyH	385	482	5227	1.9
2	MeOH	380	460	4577	0.09
	CyH	379	459	4599	0.08
3	MeOH	371	484	6293	0.3
	CyH	372	520	7651	0.65
4	MeOH	402	468	3508	0.2
	CyH	398	556	7140	3.7
5	MeOH	421	508	4068	0.1
	CyH	410	454	2364	0.17

fingerprint region (1220–1520 cm^{-1}) is dominated by ring stretching and C–H bending modes and shows significant variations with respect to substituents [Fig. 2(c) and supplementary material, Fig. S1]. A substituent effect is also seen in the low wavenumber region (especially near 500–530 cm^{-1}), which is dominated by the axle pyramidalization coupled to an H out-of-plane bending (HOOP) motion. The 517 cm^{-1} peak red-shifts, and the 536 cm^{-1} band disappears upon introduction of electron withdrawing substituents [Fig. 2(c)]. All these variations indicate that the substituents perturb the Raman active modes of the aromatic core to which they are conjugated. The nuclear displacements of the most prominent modes are illustrated in supplementary material, Fig. S1.

Time-resolved fluorescence

Time-resolved fluorescence upconversion (TRUC) measurements were performed with a 50 fs time resolution, to investigate the effect of substituents on excited state lifetimes.^{38,39} Figure 3 shows fluorescence decay dynamics of all the five motors measured, which are fitted using a sum of three exponentials function plus an offset (also shown). The complete list of decay constants are provided in Table II. Such an ultrafast non-single exponential fluorescence decay was previously observed for **3**.²³ The dominant ultrafast decay component of 100 fs and the sub-picosecond decay indicate non-single exponential relaxation of the bright Franck–Condon state to a “dark” excited state. This ultrafast step is driven by strong steric repulsion following a reduction in the axle bond order upon electronic excitation. The dark state then contributes the lower amplitude picosecond lifetime. Thus, the lower amplitude reflects the significantly reduced fluorescence transition moment for this state compared to the bright state, while its picosecond to tens of picoseconds lifetime shows that further nuclear reorganization over a potential barrier is required to access a CI with the ground electronic state.

The prompt and fastest decay component (Table II) of 100 fs (± 40 fs) assigned to bright state decay is independent of substituent. Evidently, steric repulsion dominates the fastest decay phase in 1–5. The sub-ps and few-ps decay times were previously reported for **3** to be sensitive to solvent viscosity, indicating a contribution of diffusive motion along the PES. These slower components are here also shown

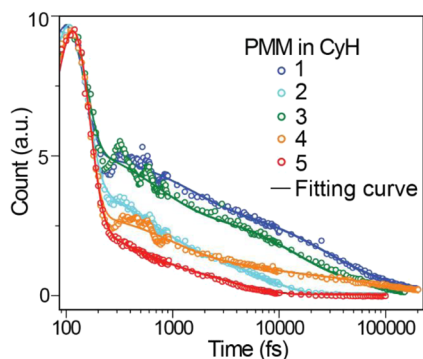


FIG. 3. Fluorescence decay of motors 1–5 with the fitted curve (black) measured near the maximum (492 nm). Note the log timescale.

TABLE II. Fluorescence decay constants and corresponding amplitudes obtained from fitting the TRUC data to a sum of three exponentials plus a fixed long component. Data were measured near the maximum wavelength of 492 nm. Typical uncertainties from repeated fitting are $\sim 20\%$.

PMM	Solvent	Upconversion time components (ps)			
1	CyH	0.1 (75%)	2.0 (9%)	27.8 (11%)	1000 (5%)
	MeOH	0.1 (81%)	1.8 (13%)	22.2 (5%)	1000 (1%)
2	CyH	0.1 (81.9%)	1.4 (10%)	8 (8%)	1000 (0.1%)
	MeOH	0.1 (87.5%)	0.9 (8.45%)	3.3 (4%)	1000 (0.05%)
3	CyH	0.1 (69%)	1.2 (13%)	17.4 (13%)	1000 (5%)
	MeOH	0.1 (76%)	1.4 (17%)	9.9 (6.8%)	1000 (0.2%)
4	CyH	0.1 (90%)	1.5 (6%)	39 (3%)	1000 (1%)
	MeOH	0.1 (95%)	1.2 (4%)	12.4 (1%)	1000 (0.001%)
5	CyH	0.1 (93%)	0.37 (3.5%)	3.2 (3.3%)	1000 (0.2%)
	MeOH	0.1 (85%)	0.44 (10%)	1.8 (4.9%)	1000 (0.1%)

to be substituent dependent (Table II). Comparing results in cyclohexane, **1** and **4** have the slowest decay for both components, which match with their higher fluorescence quantum yield (Table I). In contrast, the push–pull derivative **5** has the fastest (0.4 and 3 ps) dark state decay components. The next fastest is **2** (with a single methoxy substituent) with the unsubstituted **3** having an intermediate decay time. Note that for all derivatives, there is a minor (<5% weight) longer lived component, which is difficult to resolve accurately, so is represented here by an offset (arbitrary 1 ns component).

Clearly, in every case, the dark state decay is multi-exponential. We suggest that this arises from multiple pathways to the CI in the excited state arising from a complex landscape for both the potential energy surface and the emission transition dipole moment in the dark state. The most obvious trend in this dataset is that asymmetric substitution leads to a faster dark state decay, suggesting a lowering of the barrier to the CI in these derivatives. In all cases, a dark state decay is accelerated in polar methanol, consistent with the fluorescence quantum yield and the previous assignments of a polarity dependent barrier height.^{21,23} We note that the solvent polarity effect is modest for **1**, which also has the slowest decay, so it may be that formation of the polar structure along the reaction coordinate is less significant for the symmetric electron donating methoxy substituents. Further analysis of this substituent and solvent dependence would benefit from calculations on excited state structure and dynamics.

TRUC measurements of **1**–**5** were performed at two emission wavelengths, on the red and blue sides of the emission. As previously discussed, **3** shows a wavelength dependent emission decay with the amplitude of the fastest component decreasing on the red side of the emission (data shown in Fig. S2).²³ This represents the transition from an emissive blue-shifted bright state to a less emissive longer lived red-shifted dark state, not decay of excited state population. A similar behavior is observed for derivatives **1**, **2**, and **4** (Fig. S2),

suggesting a similar excited state mechanism. Significantly, **5** does not show any wavelength dependence in its emission decay (Fig. S2), as reported previously and assigned there to a fast (below the 50 fs time resolution) decay of the bright state.³⁶

Fluorescence coherence spectroscopy

A striking feature of the time resolved fluorescence data shown in Figs. 3 and 4(a) is the oscillations superimposed on the decay, which persist until 1 ps. The appearance of such coherent oscillations in time resolved fluorescence is indicative of vibrational dynamics, specifically in the excited electronic state, while the assignment to ground or excited state modes can be ambiguous in measurements such as ultrafast transient absorption.^{40,41} In general, two related mechanisms lead to the observed oscillations. Impulsive excitation of low frequency modes that are significantly displaced on electronic excitation leads to a modulation of the energy gap, giving rise to an oscillation at the mode frequency in the mean wavelength of the emission spectrum. In this mechanism, the transition dipole moment is assumed independent of the vibrational coordinate. In contrast, in the case that the transition dipole moment itself is a function of the coordinate, an oscillation in the spectral amplitude will be observed, called a non-Condon effect. Distinction between these two mechanisms is straightforward in wavelength resolved measurements, where the former gives rise to out-of-phase oscillations on the red and blue sides of the emission and a “phase flip” at the spectral maximum, while the non-Condon effect yields in-phase oscillations across the entire spectrum. A detailed description was presented by Ishii *et al.* in the case of transient absorption.⁴² By subtracting the fitted exponential decay, the oscillations are isolated in the residuals and may be converted to a spectral amplitude by Fourier transform [Figs. 4(b) and 4(c)]. Here, the wavelength resolved measurements show that the oscillations in the excited state are in-phase on the red and blue sides of the emission (Fig. S2), consistent with amplitude modulation, indicating a coordinate dependence of the transition dipole moment, the non-Condon effect. This result has been seen in other generations of molecular motors and for other excited state reactions.^{13,20,42} In the present case, we suggest that the non-Condon effect arises because the coherent excitation modulates progress along the bright to dark state to CI coordinate (Fig. 1), which is accompanied by a decreasing transition dipole moment.

The low frequency excited state spectra recovered from the Fourier transform are shown in Fig. 4(c). Motors **1–4** all show a well resolved band near 130–150 cm^{-1} . In addition, only motors **1** and **4** show a prominent broad peak near 50 cm^{-1} . This lower frequency band thus seems to be a feature of symmetrically substituted motors (although it is absent in the unsubstituted **3**). It is difficult to assign these low frequency features to any specific normal mode. DFT calculations for the electronic ground state predict a number of weakly Raman active modes. Typically, the nuclear motions in these modes are calculated to involve out of plane flapping of the two rings. We have not been able to correlate any specific ground state mode with the observed wavenumber (which is in the excited state) or with progress along the excited state reaction coordinate (which involves torsion and pyramidalization at the C=C bridge bond^{30,31,33}). Interestingly, **5** does not show any oscillations. We speculate that this is associated with the distinct excited state dynamics of this derivative compared to the other four, described elsewhere.³⁶

We note that for **1–4**, these low frequency modes persist in the dark-state, indicating that they survive the sterically driven ultrafast 100 fs relaxation out of the FC state. Such anharmonic nuclear motion and rapid evolution in electronic structure might be expected to lead to rapid damping of the coherently excited mode. Where coherences are observed in states that are not directly optically excited, it has been suggested that they may be impulsively excited by the ultrafast reaction itself, in this case the fast torsional dynamics.⁴³ In the present cases, the 150 cm^{-1} mode observed could, indeed, be impulsively excited by a 100 fs excited state structure change.

Femtosecond stimulated Raman spectroscopy

FSRS measurements were performed on all five motors to provide excited state vibrational spectra in the higher wavenumber region. FSRS data have not previously been reported for the first generation motors. In FSRS, an “actinic” pump pulse generates an excited state population, which is probed by a time delayed pair of pulses: a spectrally narrow Raman pump and a continuum probe. Together, these create a stimulated Raman spectrum of the transient or product states. The experiment has been described in detail elsewhere.^{11,44,45} Here, the Raman pump was fixed at 700 nm close to resonance with the bright state. Figure 5(a) shows FSRS from 400 to 1700 cm^{-1} measured 200 fs after excitation for all five motor

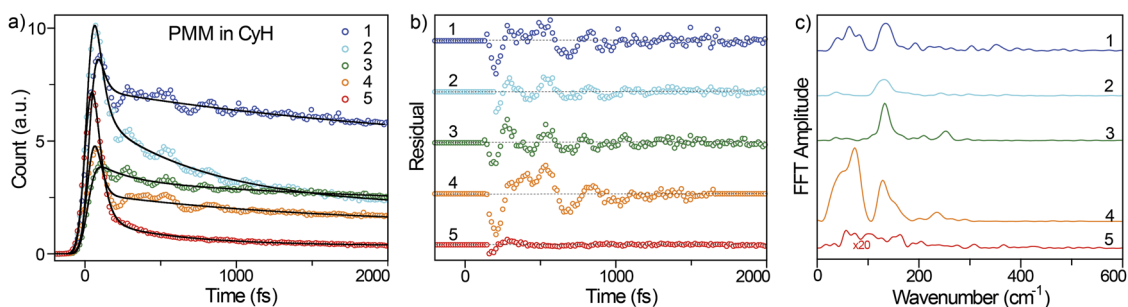


FIG. 4. (a) Fluorescence decay of motors **1–5** measured at 534 nm (red edge) with the fitted curve (black), (b) residual from the fit, and (c) Fourier transform of the residuals to give excited state coherent Raman frequencies.

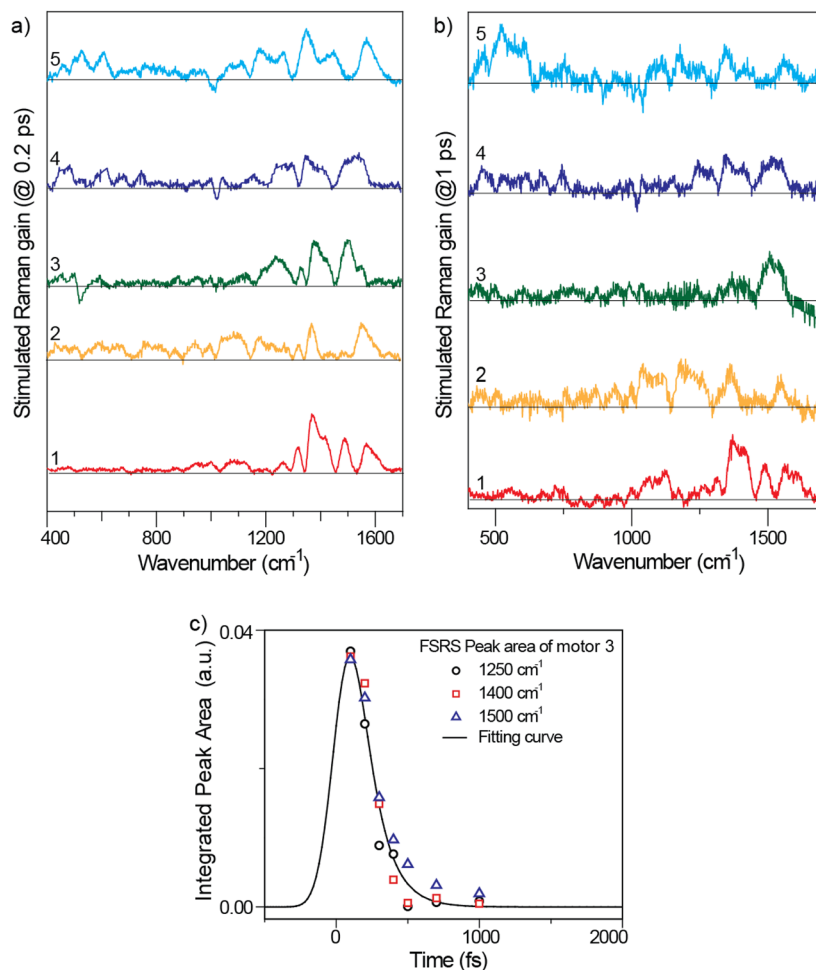


FIG. 5. Femtosecond stimulated Raman spectra of motors 1–5 at a pump–probe delay of (a) 0.2 ps and (b) 1 ps. The Raman pump was at 700 nm. (c) The measured peak area dynamics for three prominent modes of the FSRS data in motor 3 are plotted with a fitting curve of ~ 200 fs decay (black trace).

derivatives. The most intense bands are observed in the region $1300\text{--}1700\text{ cm}^{-1}$ and reveal a strong dependence on substituent. These modes are assigned based on the ground state DFT calculations to C=C stretching modes of the axle and ring. The FSRS amplitude decays rapidly, and by 1 ps, the signal to noise is poor [Fig. 5(b)]. There is little evidence of temporal evolution of the Raman spectrum on this time scale. The band area dynamics as a function of delay time for motor 3 is shown in Fig. 5(c). The fast decay of the peak area (for all three prominent peaks) with a time constant ~ 200 fs suggests that this signal corresponds to the bright state spectrum (the dark state persists for tens of picoseconds where an FSRS signal was not resolvable). From the lack of evolution and the fast decay, we can conclude that the resonant FSRS signal (with the 700 nm Raman pump wavelength employed) is dominated by the bright state. Since the population remains on the excited state surface, we assign this to an intrinsically greater stimulated Raman cross section in this state. This is in contrast to earlier studies of second generation motors where dark state FSRS was detected.^{10,20}

This most likely arises from the 700 nm Raman pump wavelength being near resonant with the very strong near IR S_1 to S_n resonance observed in bright state TA for these motors.³⁶ It is difficult to be more explicit as the specific mode enhancement depends on the in general unknown mode displacements between S_1 and S_n .^{46,47}

Comparing the highest wavenumber mode in the FSRS near $1500\text{--}1600\text{ cm}^{-1}$ (assigned to axle C=C stretching by comparison with ground state DFT), the most red-shifted band is found for the unsubstituted motor 3. Thus, all substituents, whether electron withdrawing or donating, give rise to a blue-shift [see Fig. 5(a)], which is most marked for 1 and 5. In all PMMs, the C=C stretch is at a lower wavenumber in the excited than in the ground electronic state. The broad $1100\text{--}1250\text{ cm}^{-1}$ peak in FSRS shows moderately intense signals for motors 1, 2, and 5, while that for motors 3 and 4 are weak. The low wavenumber regions show weak signals for motors 1–4, while that for motor 5 is more intense; this is in sharp contrast to the behavior at the lowest wavenumber [Fig. 4(c)], where excited state Raman activity was absent for 5. The substituent dependent

FSRS shows that the FC bright state structures are different for the five motor derivatives. Evidently, the electron donating and withdrawing substituents modify the ground and excited state electronic structures in different ways. The ground state axle C=C mode in motor **1** is the most blue-shifted, and it undergoes red-shifting in the order $2 < 3 < 4 < 5$. On the other hand, the bright state axle C=C mode in motor **3** is the most red-shifted and it undergoes blue-shifting by introducing any substituent. Interrogation of these trends by excited state calculations would yield new information on PMM excited state structure and dynamics and inform the design of more efficient motors.

CONCLUSIONS

Novel first generation PMMs have been synthesized with donor and acceptor substituents located in conjugation with the “axle” double bond. The substituents have been shown to significantly modify the photophysics, electronic structure, and vibrational spectra of both the ground and the Franck–Condon excited bright state. The effect of substituent on excited state vibrational modes is markedly different to that in the ground state. This change has been shown to correlate with changes in excited state dynamics and their sensitivity to solvent. The origin of these effects has been discussed in terms of substituent dependent electronic structures modifying the excited state reaction coordinates, especially the barrier between the dark state and the CI with the electronic ground state. Future studies of the evolution of excited state Raman spectra, along with high quality quantum dynamics calculations, will provide detailed insight into, and facilitate control over, the quantum yield of isomerization in PMMs.

SUPPLEMENTARY MATERIAL

The [supplementary material](#) contains additional experimental details, tables, and figures of DFT calculations concerning structure and vibrational spectra; further data and figures on wavelength dependent fluorescence decay and electronic spectra; and details of synthetic procedures.

ACKNOWLEDGMENTS

Financial support provided by The Netherlands Ministry of Education, Culture and Science (Gravity Program No. 024.001.035 to W.R.B. and B.L.F.) and the UKRI EPSRC (Grant Nos. EP/R042357/1 and EP/J009148/1 to SRM) is acknowledged.

AUTHOR DECLARATIONS

Conflict of Interest

The authors have no conflicts to disclose.

Author Contributions

Palas Roy: Conceptualization (lead); Formal analysis (lead); Investigation (lead); Methodology (lead); Validation (equal); Visualization

(lead); Writing – original draft (equal); Writing – review & editing (equal). **Andy S. Sardjan:** Conceptualization (equal); Investigation (equal); Methodology (equal); Resources (equal); Writing – review & editing (equal). **Wojciech Danowski:** Conceptualization (equal); Investigation (equal); Resources (lead); Visualization (equal); Writing – review & editing (equal). **Wesley R. Browne:** Conceptualization (equal); Funding acquisition (equal); Supervision (equal); Writing – review & editing (equal). **Ben L. Feringa:** Conceptualization (equal); Funding acquisition (equal); Supervision (equal); Writing – review & editing (equal). **Stephen R. Meech:** Conceptualization (equal); Funding acquisition (equal); Supervision (equal); Writing – review & editing (equal).

DATA AVAILABILITY

The data that support the findings are mainly included in the article and its [supplementary material](#) or otherwise available from the authors on reasonable request.

REFERENCES

- ¹D. R. S. Pooler *et al.*, *Chem. Sci.* **12**, 14964 (2021).
- ²D. Roke, S. J. Wezenberg, and B. L. Feringa, *Proc. Natl. Acad. Sci. U. S. A.* **115**, 9423 (2018).
- ³B. L. Feringa, *Angew. Chem., Int. Ed.* **56**, 11060 (2017).
- ⁴M. Klok, W. R. Browne, and B. L. Feringa, *Phys. Chem. Chem. Phys.* **11**, 9124 (2009).
- ⁵W. R. Browne and B. L. Feringa, *Nat. Nanotechnol.* **1**, 25 (2006).
- ⁶M. K. J. ter Wiel *et al.*, *J. Am. Chem. Soc.* **125**, 15076 (2003).
- ⁷N. Koumura *et al.*, *J. Am. Chem. Soc.* **124**, 5037 (2002).
- ⁸N. Koumura *et al.*, *Nature* **401**, 152 (1999).
- ⁹S. Amirjalayer *et al.*, *J. Phys. Chem. A* **120**, 8606 (2016).
- ¹⁰P. Roy *et al.*, *J. Phys. Chem. Lett.* **12**, 3367 (2021).
- ¹¹C. R. Hall *et al.*, *J. Am. Chem. Soc.* **139**, 7408 (2017).
- ¹²J. Conyard *et al.*, *J. Am. Chem. Soc.* **136**, 9692 (2014).
- ¹³J. Conyard *et al.*, *Nat. Chem.* **4**, 547 (2012).
- ¹⁴T. E. Wiley *et al.*, *J. Phys. Chem. A* **122**, 7548 (2018).
- ¹⁵T. Ikeda, A. G. Dijkstra, and Y. Tanimura, *J. Chem. Phys.* **150**, 114103 (2019).
- ¹⁶J. A. Berrocal *et al.*, *J. Org. Chem.* **85**, 10670 (2020).
- ¹⁷J. C. M. Kistemaker *et al.*, *J. Am. Chem. Soc.* **139**, 9650 (2017).
- ¹⁸M. M. Pollard, A. Meetsma, and B. L. Feringa, *Org. Biomol. Chem.* **6**, 507 (2008).
- ¹⁹M. Klok *et al.*, *J. Am. Chem. Soc.* **130**, 10484 (2008).
- ²⁰P. Roy *et al.*, *Nat. Commun.* **14**, 1253 (2023).
- ²¹P. Roy *et al.*, *J. Phys. Chem. A* **125**, 1711 (2021).
- ²²C. Zazza, S. Borocci, and N. Sanna, *Phys. Chem. Chem. Phys.* **26**, 5399 (2024).
- ²³A. S. Sardjan *et al.*, *ChemPhysChem* **21**, 594 (2020).
- ²⁴C. R. Hall *et al.*, *Angew. Chem., Int. Ed.* **57**, 6203 (2018).
- ²⁵X. Pang *et al.*, *J. Phys. Chem. A* **121**, 1240 (2017).
- ²⁶M. Filatov *et al.*, *Nat. Commun.* **13**, 6433 (2022).
- ²⁷A. Nikiforov *et al.*, *J. Phys. Chem. Lett.* **7**, 105 (2016).
- ²⁸M. X. Hu *et al.*, *J. Comput. Chem.* **37**, 2588 (2016).
- ²⁹M. Filatov and M. Olivucci, *J. Org. Chem.* **79**, 3587 (2014).
- ³⁰A. Kazaryan *et al.*, *J. Chem. Theory Comput.* **7**, 2189 (2011).
- ³¹A. Kazaryan *et al.*, *J. Phys. Chem. A* **114**, 5058 (2010).
- ³²Y. Y. Li *et al.*, *J. Chem. Phys.* **145**, 244311 (2016).
- ³³F. Liu and K. Morokuma, *J. Am. Chem. Soc.* **134**, 4864 (2012).
- ³⁴K. Kuntze *et al.*, *Chem. Sci.* **14**, 8458 (2023).
- ³⁵L. Pfeifer *et al.*, *Nat. Commun.* **13**, 2124 (2022).
- ³⁶P. Roy *et al.*, *J. Am. Chem. Soc.* **145**, 19849 (2023).

³⁷M. J. Frisch *et al.*, Gaussian 16 Rev C.01, Wallingford, CT, 2016.

³⁸H. Rhee and T. Joo, *Opt. Lett.* **30**, 96 (2005).

³⁹I. A. Heisler, M. Kondo, and S. R. Meech, *J. Phys. Chem. B* **113**, 1623 (2009).

⁴⁰G. Lee *et al.*, *ChemPhysChem* **18**, 670 (2017).

⁴¹J. Lee, C. H. Kim, and T. Joo, *J. Phys. Chem. A* **117**, 1400 (2013).

⁴²K. Ishii, S. Takeuchi, and T. Tahara, *J. Phys. Chem. A* **112**, 2219 (2008).

⁴³S. Y. Kim *et al.*, *J. Phys. Chem. Lett.* **3**, 2761 (2012).

⁴⁴P. Kukura, D. W. McCamant, and R. A. Mathies, *Annu. Rev. Phys. Chem.* **58**, 461 (2007).

⁴⁵P. G. Lynch *et al.*, *ACS Phys. Chem. Au* **4**, 1 (2023).

⁴⁶D. Green *et al.*, *J. Phys. Chem. A* **125**, 6171 (2021).

⁴⁷M. S. Barclay *et al.*, *J. Phys. Chem. A* **121**, 7937 (2017).